composite NusA–β-subunit surface with RNA may stabilize RNA structures and explain NusA's ability to accelerate cotranscriptional folding of RNA (25).

How might an allosteric signal generated by flap contact affect catalysis in the active site, which is 65 Å from the flap-tip helix? The flap domain connects to RNAP through a two-stranded, antiparallel β sheet (the connector). The connector runs along the active-site cleft to highly conserved amino acids in the active site (E813, D814, and K1065; Fig. 2). E813 and D814 may chelate the Mg^{2+} ion bound to the substrate nucleoside triphosphate (NTP); K1065 contacts the α phosphate of the 3'-terminal RNA nt; substitution of E813 or K1065 disrupts catalysis (26, 27). Therefore, the pause hairpin may affect catalysis by moving the flap and, by way of the connector, critical residues in RNAP's active site. Alternatively, hairpin formation could open the active-site cleft by moving the clamp domain. Conversely, flap or clamp movement and possibly hairpin formation could be inhibited when NTPs bind efficiently (because bound NTP would constrain the position of E813/D814), and may be coupled to movements of parts of RNAP that form the active-site cleft and downstream DNA jaws (Fig. 2) (13).

Definition of the flap-tip helix as an allosteric site on RNAP provides a new framework for understanding RNAP's regulation. σ also binds RNAP's flap (28); σ may open the RNA exit channel to thread RNA into the channel; σ release may allow the channel to close for efficient transcript elongation (13). Like pause hairpins, terminator hairpins probably also open the RNA exit channel, rather than pull RNA out of RNAP, and then dissociate the TEC by invading the RNA:DNA hybrid, opening the active-site cleft, and triggering collapse of the transcription bubble (3, 6). Finally, eukaryotic RNAPs also contain a flap domain, making the flap an attractive target for both prokaryotic and eukaryotic regulators of transcription.

References and Notes

1. G. Zhang et al., Cell 98, 811 (1999).
2. P. Cramer et al., Science 288, 640 (2000).
3. N. Korzheva et al., Science 289, 619 (2000).
4. E. Nudler, A. Mustaev, E. Lukhtanov, A. Goldfarb, Cell 89, 33 (1997).
5. I. Sidorenkov, N. Komissarova, M. Kashlev, Mol. Cell 2, 55 (1998).
6. I. Artsimovitch, R. Landick, Genes Dev. 12, 3110 (1998).
7. W. S. Yarnell, J. W. Roberts, Science 284, 611 (1999).
8. C. L. Chan, R. Landick, J. Mol. Biol. 233, 25 (1993).
9. C. D. Sigmund, E. A. Morgan, Biochemistry 27, 5622 (1988).
10. P. J. Farnham, T. Platt, Cell 20, 739 (1980).
11. T. D. Yager, P. H. von Hippel, Biochemistry 30, 1097 (1991).
12. I. Gusarov, E. Nudler, Mol. Cell 3, 495 (1999).
13. R. A. Mooney, R. Landick, Cell 98, 687 (1999).
14. R. J. Davenport, G. J. Wuite, R. Landick, C. Bustamante, Science 287, 2497 (2000).
15. I. Artsimovitch, R. Landick, Proc. Natl. Acad. Sci. U.S.A. 97, 7090 (2000).
16. The his pause synchronizes transcription with trans-lation in the attenuation control region of the E. coli his operon (8). The pause signal is multipartite; interactions of downstream DNA, 3'-proximal RNA, and NTP substrate, together with the pause hairpin, inhibit nucleotide addition by a factor of ~100 (8).
17. D. Wang, K. Severinov, R. Landick, Proc. Natl. Acad. Sci. U.S.A. 94, 8433 (1997).
18. E. Ennifar et al., J. Mol. Biol. 304, 35 (2000).
19. Supplementary data are available on Science Online at www.sciencemag.org/cgi/content/full/292/5517/730/DC1.
20. K. Meisenheimer, T. Koch, Crit. Rev. Biochem. Mol. Biol. 32, 101 (1997).
21. RNAP subunits (α, NH_2-terminally His_6-tagged wild-type or mutant β, and β' carrying a COOH-terminal intein and chitin-binding domain) were co-overexpressed in E. coli. After sonication and capture of RNAP on a chitin matrix (New England Biolabs), RNAP was recovered by dithiothreitol-mediated intein cleavage. βF934A RNAP paused equivalently to wild-type RNAP; βF906A RNAP pausing was more sensitive to competition by Cl⁻; βΔ(900-909) RNAP pausing was reduced at both low and high [Cl⁻] (Fig. 4). TEC synthesis and photocross-linking were performed as described (17).
22. R. D. Finn, E. V. Orlova, B. Gowen, M. Buck, M. van Heel, EMBO J. 19, 6833 (2000).
23. D. N. Lee, R. Landick, J. Mol. Biol. 228, 759 (1992).
24. C. Chan, D. Wang, R. Landick, J. Mol. Biol. 268, 54 (1997).
25. T. Pan, I. Artsimovitch, X. W. Fang, R. Landick, T. R. Sosnick, Proc. Natl. Acad. Sci. U.S.A. 96, 9545 (1999).
26. A. Mustaev et al., J. Biol. Chem. 266, 23927 (1991).
27. V. Sagitov, V. Nikiforov, A. Goldfarb, J. Biol. Chem. 268, 2195 (1993).
28. T. Gruber, I. Artsimovitch, K. Geszvain, R. Landick, C. Gross, unpublished data.
29. We thank S. Darst for help in molecular modeling and pointing out the possible role of βED813/814; K. Murakami for sharing an RNAP overexpression plasmid; M. Barker, R. Gourse, R. Saecker, M. Sharp, and members of our lab for helpful suggestions; and the NIH for support (GM38660).

Reversible Unfolding of Single RNA Molecules by Mechanical Force

Jan Liphardt,[1] Bibiana Onoa,[1] Steven B. Smith,[2] Ignacio Tinoco Jr.,[1] Carlos Bustamante[1,2]*

Here we use mechanical force to induce the unfolding and refolding of single RNA molecules: a simple RNA hairpin, a molecule containing a three-helix junction, and the P5abc domain of the Tetrahymena thermophila ribozyme. All three molecules (P5abc only in the absence of Mg^{2+}) can be mechanically unfolded at equilibrium, and when kept at constant force within a critical force range, are bi-stable and hop between folded and unfolded states. We determine the force-dependent equilibrium constants for folding/unfolding these single RNA molecules and the positions of their transition states along the reaction coordinate.

RNA molecules must fold into specific three-dimensional shapes to perform catalysis. However, bulk studies of folding are often frustrated by the presence of multiple species and multiple folding pathways, whereas single-molecule studies can follow folding/unfolding trajectories of individual molecules (1). Furthermore, in mechanically induced unfolding, the reaction can be followed along a well-defined coordinate, the molecular end-to-end distance (x).

We studied three types of RNA molecules representing major structural units of large RNA assemblies. P5ab (Fig. 1A) is a simple RNA hairpin that typifies the basic unit of RNA structure, an A-form double helix. P5abcΔA has an additional helix and thus a three-helix junction. Finally, P5abc is comparatively complex and contains an A-rich bulge, enabling P5abc to pack into a stable tertiary structure (a metal-ion core) in the presence of Mg^{2+} ions (2–9).

The individual RNA molecules were attached to polystyrene beads by RNA/DNA hybrid "handles" (Fig. 1B) (10). One bead was held in a force-measuring optical trap, and the other bead was linked to a piezo-electric actuator through a micropipette (11, 12). When the handles alone were pulled, the force increased monotonically with extension (Fig. 2A, red line), but when the handles with the P5ab RNA were pulled, the force-extension curve was interrupted at 14.5 pN by an ~18-nm plateau (black curve), consistent with complete unfolding of the hairpin. The force of 14.5 pN is similar to that required to unzip DNA helices (13, 14). P5ab switched from the folded to the unfolded state, and vice-versa, in less than 10 ms and without intermediates. Forward and reverse curves nearly coincided, indicating thermal equilibrium. The variation of folding/unfolding force (SD 0.4 pN) reflects the stochastic nature of a thermally facilitated process. Indeed, a plot of the fraction unfolded versus force (Fig. 2B, dots) is fit well by the statistics of a two-

[1]Department of Chemistry and [2]Departments of Physics and Molecular and Cell Biology, Howard Hughes Medical Institute, University of California, Berkeley, CA 94720, USA.

*To whom correspondence should be addressed. E-mail: carlos@alice.berkeley.edu

state system in an external field at finite temperature (solid line). From this analysis, P5ab's unfolding free energy (ΔG) is 193 ± 6 kJ mol^{-1} (12, 15). A second, independent, measure of P5ab's ΔG is the average area under the reversible folding/unfolding plateau, which equals the potential of mean force of folding and yields a ΔG of 157 ± 20 kJ mol^{-1}. After correction for the free energy reduction of the unfolded state due to tethering (calculated to be 44 ± 10 kJ mol^{-1}) (12), these values compare well with the predicted ΔG of unfolding untethered P5ab calculated with the *mfold* free energy–minimization method ($\Delta G_{\text{sigmoid}}$ = 149 ± 16; $\Delta G_{\langle\text{area}\rangle}$ = 113 ± 30; ΔG_{mfold} = 147 kJ mol^{-1}) (12, 16).

Several force-extension traces showed the molecule's extension jumping between two values when the force was within ~1 pN of the unfolding plateau (Fig. 2A, left inset). We investigated this bi-stability by imposing a constant force on the molecule with feedback-stabilized optical tweezers capable of maintaining a preset force within ±0.05 pN by moving the beads closer or further apart. Then, the end-to-end distance of the P5ab hairpin hopped back and forth by ~18 nm, signaling the repeated folding and unfolding of a single RNA molecule. As in the pulling experiments, transitions between the two states were unresolvably fast (<10 ms) and without intermediates. By increasing the pre-set force, it was possible to tilt the folded⇔unfolded equilibrium toward the unfolded state and thus directly to control the thermodynamics and kinetics of RNA folding in real time (Fig. 2C). As the force was increased, the molecule spent more time in the extended open form and less time in the short folded form.
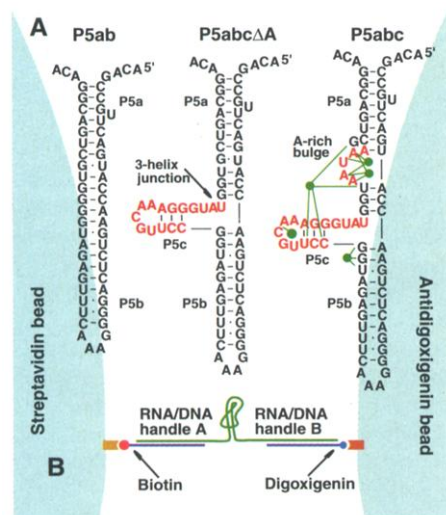
Whether hopping can be observed with a particular type of RNA depends on the time resolution of the instrument, its drift rate, and the kinetic barrier to folding/unfolding as determined by the potential energy surface of the molecule (12). In the instrument we used, hopping could be observed for rates between approximately 0.05 Hz and 20 Hz.

A ratio of the average lifetimes of the molecule in the two states yields the equilibrium constant $K(F)$ for folding/unfolding at that force (Fig. 2D). Linear extrapolation of $K(F)$ to zero force, and correction for free energy reduction due to tethering (as above), yields a ΔG of 156 ± 8 kJ mol^{-1}, which coincides with the ΔG values obtained from stretching and the predicted value. Therefore, three different methods of measuring P5ab's unfolding ΔG give similar results: (i) the fit to the distribution of opening forces, (ii) the average area under the folding/unfolding plateau, and (iii) the ratio of folded and unfolded lifetimes.

The sensitivity of RNA hopping to external force is determined by the force-dependent length difference between the unfolded and folded forms, $\Delta x(F)$. In particular, an expression analogous to the van't Hoff formula holds: $d \ln K (F)/dF = \Delta x(F)/k_B T$ (17). Indeed, the slope of the ln K versus F plot (Fig. 2D) multiplied by $k_B T$ is 23 ± 4 nm, and the $\Delta x(F_{1/2})$ value thus obtained is within experimental error of the value from the
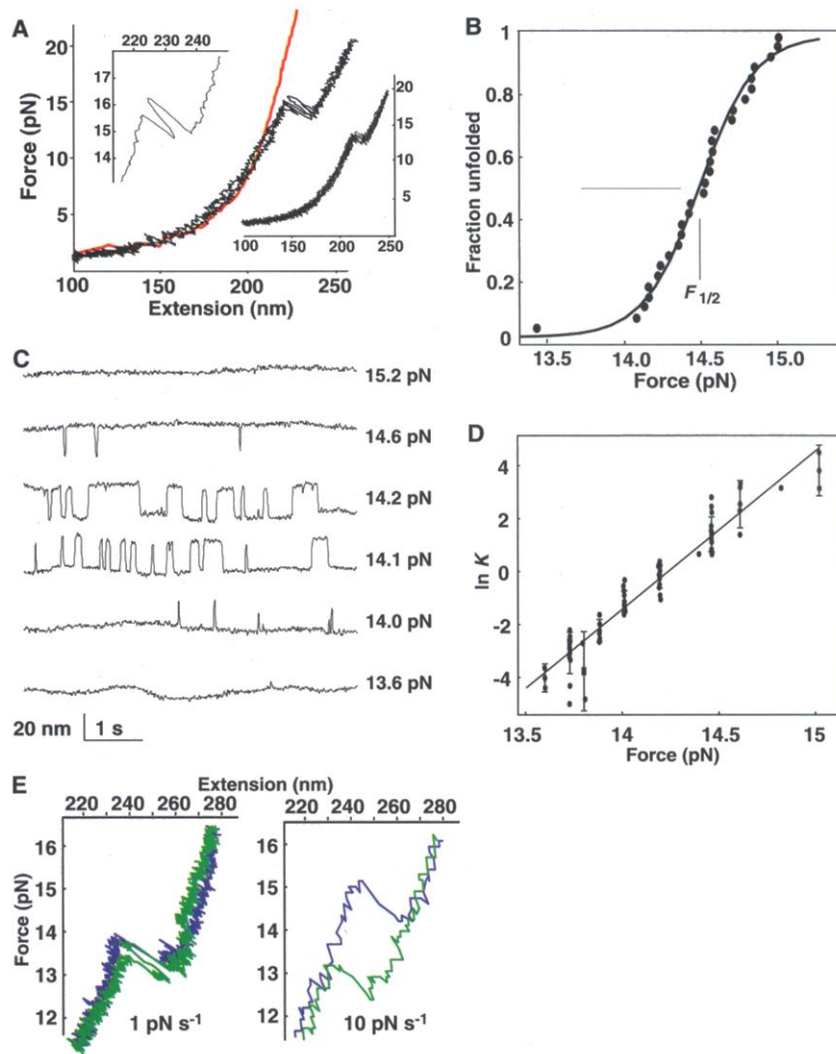

Fig. 1. (A) Sequence and secondary structure of the P5ab, P5abcΔA, and P5abc RNAs. The five green dots represent magnesium ions that form bonds (green lines) with groups in the P5c helix and the A-rich bulge (3). (B) RNA molecules were attached between two 2-μm beads with ~500–base pair RNA:DNA hybrid handles.

Fig. 2. (A) Force-extension curves of the RNA-DNA handles without an insert (red) and with the P5ab RNA (black) in 10 mM Mg^{2+}. Stretching and relaxing curves are superimposed. Inset, detail of force-extension trace showing hopping. Right inset, force-extension curve for the RNA hairpin without Mg^{2+}. (B) Probability of opening versus force in Mg^{2+} was obtained by summing a normalized histogram of hairpins opened versus force. Data are from 36 consecutive pulls of one molecule. Solid line, probability $p(E)$ of a two-state system: $p(E) = 1 (1 + e^{E/k_B T})$. Best-fit (least squares) values, $\Delta G(F_{1/2}) = 193 ± 6$ kJ mol^{-1}, $\Delta x = 22 ± 1$ nm (12). (C) Length versus time traces of the RNA hairpin at various constant forces in 10 mM Mg^{2+}. (D) The logarithm of the equilibrium constant in Mg^{2+} plotted as a function of force (error bar = 1 SD). (E) Detail of the stretching (blue) and relaxing (green) force-extension curves of the P5abcΔA molecule taken at low and high loading rates in 10 mM Mg^{2+}.

length-time trace (18 ± 2 nm, Table 1) (*18*).

P5ab's folding kinetics in Mg^{2+} were determined from the force-dependent average lifetimes of the folded and unfolded forms, $\langle\tau_f\rangle$ and $\langle\tau_u\rangle$ (Fig. 2C). The logarithm of the mechanical folding/unfolding rate appears to be a linear function of external force, with $k_{f\to u}$ increasing from 0.5 s^{-1} to 30 s^{-1} with force, and $k_{u\to f}$ decreasing from 30 s^{-1} to 0.4 s^{-1} (Table 1) (*12*). These rate constants then can be fit to Arrhenius-like expressions of the form:

$$k_{f\to u}(F) = k_m k_0 e^{F\Delta x^{\ddagger}_{f\to u}/k_B T} \qquad (1)$$

where k_m represents the contribution of handle and bead fluctuations to the absolute rates (*19*), k_0 is the RNA's unfolding rate at zero force, and $\Delta x^{\ddagger}_{f\to u}$ is the thermally averaged distance between the folded state and the transition state along the direction of force (*20*). A similar expression holds for the reverse reaction. Consistent with the predicted shape of P5ab's free energy curve along the reaction coordinate (*12*), the position of P5ab's transition state on the reaction coordinate determined from the slope of the ln k versus F plots is equidistant from the unfolded and folded states: $\Delta x^{\ddagger}_{u\to f} = 11.5$ nm, and $\Delta x^{\ddagger}_{f\to u} = 11.9$ nm. By contrast, the transition state for mechanical unfolding of certain protein domains, e.g., titin immunoglobulin, is closer to the native state (~0.3 nm) than the denatured state (between 2 and 8 nm) (*21, 22*). These positioning differences may reflect the absence of nonlocal (tertiary) contacts in the P5ab hairpin and the dependence of the stability of the protein-folded state on nonlocal interactions.

Removal of Mg^{2+} lowers the average force of folding/unfolding in pulling experiments from 14.5 to 13.3 pN, thus reducing the $\Delta G_{\langle area\rangle}$ by 8%. It does not, however, affect the transition state position on the reaction coordinate (Table 1). Mg^{2+} thus slightly stabilizes the P5ab hairpin, presumably through nonspecific ionic shielding of phosphate repulsions (*23, 24*).

Having explored the simplest RNA structural unit, we characterized the mechanical behavior of a helix junction. The P5abcΔA three-helix junction (Fig. 1A) also hopped between two states when held at constant force in Mg^{2+} and EDTA (Table 1). However, a force-hysteresis of ~1.5 pN was observed in the force-extension curves in both ionic conditions, indicating a loading rate faster than the slowest relaxation process of the molecule. Thermodynamic equilibrium, as marked by coincident stretch and relax curves, was attained when loading rates (*20*) were reduced to ≤1 pN s^{-1} (Fig. 2E). The rates of P5abcΔA's folding/unfolding are smaller than those of P5ab, despite identical effective transition state location, presumably because two hairpins must nucleate, and therefore, two kinetic barriers, representing two transition states, must be crossed to fold P5abcΔA. Similarly, two helices must be opened sequentially to unfold P5abcΔA. The overall activation barrier for P5abcΔA folding/unfolding is therefore larger than that of P5ab, slowing its kinetics.

Although helices and their combinations are fundamental units of RNA structure, they are not sufficient for three-dimensional organization. Consequently, we investigated Mg^{2+}-dependent tertiary contacts using the P5abc RNA, whose structure is stabilized by Mg^{2+} ions that form a metal-ion core between the P5c helix and the A-rich bulge (Fig. 1A) (*3*).

As shown in Fig. 3A, the tertiary interactions formed in Mg^{2+} lead to substantial curve hysteresis (loading rate: 3 pN s^{-1}). Forces as high as 22 pN are needed before the molecule suddenly unfolds (blue curves), displaying a "molecular stick-slip" or "ripping" behavior (*25*). Typically, the molecule unfolds suddenly at a high force (19 ± 3 pN, 96% of curves, $n = 150$, Fig. 3A, blue arrow). Rarely (4% of curves), unfolding is interrupted after 13 nm, and the force then rises again until a second rip (inset, red stars) completes unfolding. The two-step unfolding reveals two distinct kinetic barriers to mechanical unfolding of P5abc in Mg^{2+}. Considering the ionic requirements of those barriers (see below), and their absence in the P5ab and P5abcΔA curves, we assign them to Mg^{2+}-dependent tertiary interactions among the P5c helix, the A-rich bulge, and the rest of the molecule. Because it is not preceded by other unfolding, the first rip must represent opening of P5a followed by rip propagation through the entire RNA structure (Fig. 3F, most probable path, blue arrow). Unfolding is sometimes interrupted by the second barrier, probably located at

Table 1. Force-extension and constant force measurements.

		Force-extension measurements (298 K)			
Molecule	No. of nucleotides	ΔG (kJ/mol) Mfold[16]	$F_{1/2}$ (pN) of unfolding	$\Delta x_{1/2}$ (nm) of plateaus/rips	$\Delta G_{1/2}$ (kJ/mol) $F_{1/2}\Delta\cdot x_{1/2}$
P5ab, Mg^{2+}	49	147	14.5 ± 1	18 ± 2	157 ± 20
P5ab, EDTA	49	147	13.3 ± 1	18 ± 2	144 ± 20
P5abcΔA, Mg^{2+}	64	174	12.7 ± 0.3	22 ± 3	169 ± 27
P5abcΔA, EDTA	64	174	11.4 ± 0.5	21 ± 2	144 ± 20
P5abc[1], Mg^{2+}	69	152	8–22	13, 14, 26	–
P5abc[2], EDTA	69	152	7–11	26 ± 3	140

		Constant force measurements (298 K)[4]		
Molecule	$\langle\Delta x\rangle$ (nm)[3]	ln K vs. force (pN)[4]	ln $k(s^{-1})$ vs. force (pN) (SS to hairpin)[4]	ln $k(s^{-1})$ vs. force (pN) (hairpin to SS)[4]
P5ab, Mg^{2+}	19 ± 2	$-81 \pm 3.5 + (5.7 \pm 0.2)F$	$41 \pm 1.9 - (2.8 \pm 0.1)F$	$-39 \pm 2.3 + (2.9 \pm 0.2)F$
P5ab, EDTA	18 ± 2	$-69 \pm 4.4 + (5.3 \pm 0.4)F$	$37 \pm 4.0 - (2.7 \pm 0.3)F$	$-32 \pm 4.8 + (2.6 \pm 0.4)F$
P5abcΔA, Mg^{2+}	22 ± 4	$-98 \pm 9.5 + (6.9 \pm 0.7)F$	$58 \pm 7.5 - (4.2 \pm 0.5)F$	$-39 \pm 9.3 + (2.7 \pm 0.7)F$
P5abcΔA, EDTA	23 ± 2	$-63 \pm 14 + (5.1 \pm 1.2)F$	$31 \pm 6.0 - (2.6 \pm 0.5)F$	$-31 \pm 11 + (2.5 \pm 0.3)F$
P5abc[5], Mg^{2+}	26 ± 3			$-8.5 \pm 0.7 + (0.4 \pm 0.02)F[6]$
P5abc[7], EDTA	17 ± 2			

[1]P5abc's unfolding is not reversible in Mg^{2+}. These values are the forces and length-changes of the unfolding rips. [2]Folding/unfolding was not two-state. The change in length between the folded and unfolded states was determined by measuring the total offset of the pulling curve following complete unwinding of P5abc. [3]From the extension time trace. [4]The change in the end-to-end distance across the transition, and thus the slope of the ln K and ln k versus force plots, is force-dependent. The force dependence of Δx and $\Delta x^{\ddagger}$ may be neglected for small differences of force but based on the WLC model (*12*) they will need to be taken into account when extrapolating to zero-force. Also, the relative position of the transition state on the reaction coordinate may be force-dependent. [5]P5abc does not hop in the presence of Mg^{2+}. [6]From the fits of the varible-rate experiments (Fig. 3C). [7]P5abc's hopping in EDTA is not two-state.

the base of the P5b helix (Fig. 3F, rare path, red arrow). Consistent with the slow kinetics of P5abc in Mg^{2+} (Fig. 3A), these molecules do not hop when held at constant force; rather, they unfold suddenly and do not refold for the duration of the experiment (5 min, Fig. 3E).

Removal of Mg^{2+} removes the kinetic barriers, and folding/unfolding becomes reversible. Unfolding then begins at 7 pN (Fig. 3B), showing that in EDTA the A-rich bulge destabilizes P5abc. The refolding curves in Mg^{2+} and EDTA coincide, except for an offset of 1.5 pN due to charge neutralization (Fig. 3B, green curves). In contrast to the all-or-none behavior of P5ab, refolding of P5abc both with and without Mg^{2+} has intermediates: the force curve inflects gradually between 14 and 11 pN (Fig. 3B, black stars) and this inflection is followed by a fast (<10 ms) hop without intermediates at 8 pN (green arrows). The cooperativity of mechanically induced folding/unfolding is determined by the shape of the free-energy surface along the reaction coordinate and, thus, by the RNA sequence (12).

The different widths of the two transitions and their force-separation suggest that the inflection (Fig. 3B, stars) marks folding of the P5b/c helices, whereas the hop (Fig. 3B, arrows) marks P5a helix formation. The folding/unfolding of P5a as compared with P5b/c can be resolved in constant-force experiments. Now, although the molecule hops (Fig. 3D), the average length of its hops (~17-nm) is only about two-thirds the expected value, and a second type of hop is occasionally observed (red arrow) (12). Evidently, in EDTA P5abc hops between partially folded states, with the ~17 nm transitions presumably representing folding/unfolding of the P5a helix and parts of the three-helix junction.

To measure P5abc's unfolding kinetics in Mg^{2+}, we determined the probability that the molecule will be unfolded (ripped) at a given force from a series of unfolding curves like Fig. 3A (blue). From these data, the unfolding rate and the position of the transition state of the first barrier were obtained using (20):

$$N(F,r) = e^{\frac{k_m k_0}{br}(e^{bF}-1)} \qquad (2)$$

In the high-force limit (>3 pN), this expression may be simplified to the following:

$$\ln\{r\ln[1/N(F,r)]\} = \ln(k_m k_0/b) + bF \qquad (3)$$

where N is the fraction folded, r is the loading rate (pN s^{-1}), k_0 is the zero-force opening rate, and $b = \Delta x^{\ddagger}/k_B T$. Plots of the $\ln[r\ln(1/N)]$ versus force for the first barrier at loading rates of 1 and 10 pN s^{-1} are shown in Fig. 3C. A fit of the data in Fig. 3C yields a distance of 1.6 ± 0.1 nm from the folded to the transition state ($\Delta x^{\ddagger}_{f\rightarrow u}$) along the reaction coordinate, and an apparent k_0 of 2×10^{-4} s^{-1}. Thus the A-rich bulge, in the presence of Mg^{2+}, converts an RNA with a $\Delta x^{\ddagger}_{f\rightarrow u}$ of 12 nm (P5abcΔA), into one with a transition distance similar to those of globular proteins. Apparently, the nonlocal contacts in hydrophobic and electrostatic cores of proteins and RNAs, respectively, are responsible for their cooperative unfolding behavior under locally applied mechanical forces.

How does the metal-ion core stabilize P5abc against mechanical unfolding? The $\Delta G^{\ddagger}$ of opening P5abc's tertiary contact is about 80 kJ mol^{-1} smaller than the $\Delta G^{\ddagger}$ of opening the P5ab and P5abcΔA helices (zero-force rate: 10^{-4} versus 10^{-18}, Table 1). Why then is opening P5abc's tertiary contact, and not its helices, rate limiting to mechanical unfolding? At any finite pulling rate, and for a given $\Delta G^{\ddagger}$, the average force required to commence unfolding is inversely proportional to $\Delta x^{\ddagger}_{f\rightarrow u}$, which, for the tertiary contact, is 7 times as short as for a helix. P5abc in Mg^{2+} is consequently a "brittle" structure that resists mechanical deformation but fractures once deformed slightly. Conversely, the P5ab helix is compliant and unfolds reversibly under mechanical force.

Unlike the secondary structural elements of proteins, those of RNA are independently stable. The free energies of secondary and tertiary interactions of RNA may therefore be additive and separable. By revealing these free energies, mechanical and fluorescence studies (1) of individual RNAs will help develop an *aufbau* algorithm for RNA folding (26). Mechanical studies permit uninterrupted access (lasting
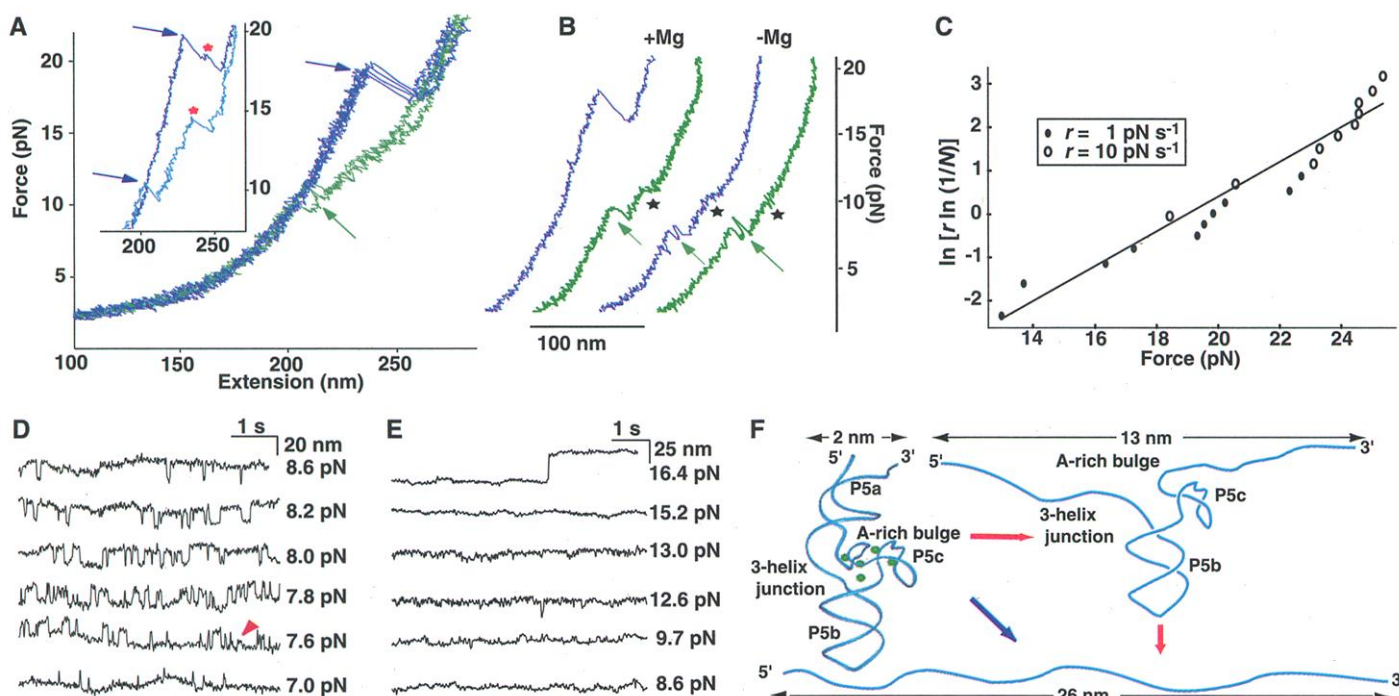

Fig. 3. (A) Stretch (blue) and relax (green) force-extension curves for P5abc in 10 mM Mg^{2+}. Inset, detail of P5abc stretching curves showing unfolding intermediates (red stars). (B) Comparison of P5abc force-extension curves in the presence and absence of Mg^{2+}. (C) The force-distribution of unfolding of the first kinetic barrier at loading rates of 1 and 10 pN s^{-1}. Best fit (least squares) values, $\Delta x_{f\rightarrow u} = 1.6 \pm 0.1$ nm, $k_0 = 2 \times 10^{-4}$ s^{-1}. (D) Length versus time traces for P5abc in EDTA (12). (E) Length versus time traces of P5abc in 10 mM Mg^{2+}. (F) Model for P5abc's unfolding by force in Mg^{2+}.

minutes to hours) to the kinetic and thermodynamic properties of single polymers; investigation of folding/unfolding in physiological ionic strengths and temperatures; and determination of the effects of ions, drugs, and proteins on RNA structure (27).

References and Notes
1. X. Zhuang et al., Science **288**, 2048 (2000).
2. J. H. Cate et al., Science **273**, 1678 (1996).
3. J. H. Cate, R. L. Hanna, J. A. Doudna, Nature Struct. Biol. **4**, 553 (1997).
4. D. K. Treiber, J. R. Williamson, Curr. Opin. Struct. Biol. **9**, 339 (1999).
5. A. R. Ferre-D'Amare, J. A. Doudna, Annu. Rev. Biophys. Biomol. Struct. **28**, 57 (1999).
6. A. M. Pyle, Science **261**, 709 (1993).
7. M. Wu, I. Tinoco Jr., Proc. Natl. Acad. Sci. U.S.A. **95**, 11555 (1998).
8. C. Y. Ralston, Q. He, M. Brenowitz, M. R. Chance, Nature Struct. Biol. **7**, 371 (2000).
9. J. Pan, D. Thirumalai, S. A. Woodson, Proc. Natl. Acad. Sci. U.S.A. **96**, 6149 (1999).
10. The DNA-RNA hybrid molecules were prepared by annealing the ends of a ~1.2-kb RNA to complementary DNA molecules (12). Pulling experiments were performed at 298 K in 10 mM Tris, 250 mM NaCl, and either 10 mM $MgCl_2$ or EDTA.
11. S. B. Smith, Y. Cui, C. Bustamante, Science **271**, 795 (1996).
12. Supplementary material is available on Science Online at www.sciencemag.org/cgi/content/full/292/5517/733/DC1.
13. B. Essevaz-Roulet, U. Bockelmann, F. Heslot, Proc. Natl. Acad. Sci. U.S.A. **94**, 11935 (1997).
14. M. Reif, H. Clausen-Schaumann, H. Gaub, Nature Struct. Biol. **6**, 346 (1999).
15. Unless indicated otherwise, free energies are valid for a force of $F_{1/2}$, 298 K, and 250 mM NaCl, 10 mM Mg^{2+}.
16. M. Zuker, Curr. Opin. Struct. Biol. **10**, 303 (2000).
17. J. G. Kirkwood, I. Oppenheim, Chemical Thermodynamics (McGraw-Hill, New York, 1961).
18. $\Delta x(F_{1/2}) = \Delta x_{1/2}$ was obtained from plots of $\ln K_{eq}(F)$ versus force using $d\ln K_{eq}(F)/dF = \Delta x(F)/k_B T$, where $\Delta x(F)$ was expanded as $\Delta x_{1/2} + (F - F_{1/2})dx/dF$. The WLC model gives (high-force limit) $dx/dF = L(4F\sqrt{FP/k_B T})^{-1}$.
19. The measured rate constants are the rates with which the entire system (beads, handles, and RNA) hops from one extension to another. The various contributions are expressed in Eq. 1 as the product of a "machine" constant k_m and a molecule constant k_0. Therefore, hopping reveals the sensitivity of RNA folding/unfolding to external force (the distance to the transition state $\Delta x^{\ddagger}$) and the difference between the $\Delta G^{\ddagger}$ values (the ΔG of unfolding), but not the absolute rates or $\Delta G^{\ddagger}$ values (12).
20. E. Evans, K. Ritchie, Biophys. J. **72**, 1541 (1997).
21. M. Carrion-Vazquez et al., Proc. Natl. Acad. Sci. U.S.A. **96**, 3694 (1999).
22. M. S. Kellermayer, S. B. Smith, H. L. Granzier, C. Bustamante, Science **276**, 1112 (1997).
23. C. Ma, V. A. Bloomfield, Biopolymers **35**, 211 (1995).
24. V. K. Misra, D. E. Draper, Biopolymers **48**, 113 (1998).
25. U. Bockelmann, B. Essavez-Roulet, F. Heslot, Phys. Rev. **E58**, 2386 (1998).
26. I. Tinoco Jr., C. Bustamante, J. Mol. Biol. **293**, 271 (1999).
27. This research was supported in part by NIH grants GM-10840 and GM-32543, Department of Energy grants DE-FG03-86ER60406 and DE-AC03-76SF00098, and NSF grants MBC-9118482 and DBI-9732140. J.T.L. is supported by the Program in Mathematics and Molecular Biology through a Burroughs Wellcome Fund Fellowship.

20 December 2000; accepted 13 March 2001

Switching Repulsion to Attraction: Changing Responses to Slit During Transition in Mesoderm Migration

Sunita G. Kramer, Thomas Kidd,* Julie H. Simpson, Corey S. Goodman†

Slit is secreted by cells at the midline of the central nervous system, where it binds to Roundabout (Robo) receptors and functions as a potent repellent. We found that migrating mesodermal cells in vivo respond to Slit as both an attractant and a repellent and that Robo receptors are required for both functions. Mesoderm cells expressing Robo receptors initially migrate away from Slit at the midline. A few hours after migration, these same cells change their behavior and require Robo to extend toward Slit-expressing muscle attachment sites. Thus, Slit functions as a chemoattractant to provide specificity for muscle patterning.

Migrating cells are guided by attractive and repulsive signals (1). Many of these factors are bifunctional (1–5). In addition, migrating cells can switch on or off their responsiveness to particular guidance cues (6–8). In vitro, growth cones can switch between attraction and repulsion if the internal state of the cell is altered [e.g., (9, 10)]. Here we show that such a change takes place in the developing mesoderm in the Drosophila embryo. Migrating mesodermal cells switch their responsiveness to Slit as they switch phases in their differentiation. Initially, they are repelled by Slit

emanating from the midline, but only a few hours later, they are attracted to Slit secreted by epidermal muscle attachment sites (MASs).

The first phase of cell migration during Drosophila myogenesis occurs after gastrulation, when muscle precursor cells migrate through the ventral furrow and spread dorsally to coat the inner surface of the ectoderm. In the second phase, muscle precursors fuse to form individual muscle fibers as they extend growth cone–like processes, which migrate toward specific MASs within the epidermis (11–13).

The migration of the mesodermal cells that will form ventral muscles is dependent on the expression of Slit, an extracellular matrix molecule secreted by midline cells (14). In slit mutant embryos, many ventral muscle precursors fail to migrate away from the midline and fuse to form muscles that

inappropriately stretch across the central nervous system (CNS) (Fig. 1B) (15, 16). On the basis of staining with several muscle-specific markers, we identified most of these misplaced muscles as ventral muscles 6 and 7 (17). These defects are rescued by expressing UAS-slit at the ventral midline using single-minded-GAL4 (18), confirming that the midline expression of Slit is required for the migration of muscle precursors away from this region (Fig. 1D) (16).

In the Drosophila CNS, Slit is the repulsive ligand for the Roundabout (Robo) family of receptors (7, 15, 19–23). The Drosophila genome encodes three Robo receptors: Robo, Robo2, and Robo3. Robo and Robo2 together control repulsive axon guidance at the midline (20, 22). The repulsion of mesodermal cells by Slit at the midline also requires Robo and Robo2. In robo mutant embryos, occasional muscles can be seen crossing the midline (15, 16), whereas in the robo,robo2 double mutant, the muscle phenotype resembles that of slit, with most segments containing multiple muscles 6 and 7 stretched across the midline (Fig. 1C) (16). This defect can be rescued by expressing either a robo or robo2 transgene in all muscles with the 24B-GAL4 driver (18).

After their migration away from the midline, specific muscle precursor cells fuse with neighboring myoblasts to form muscle fibers (11, 24). These muscles extend growth cone–like processes toward their appropriate MASs (12, 13). Little is known about the cues that guide these cell-specific migrations. Here we show that Slit is one of these cues, but in this case, Slit functions as an attractant for muscles expressing Robo and/or Robo2.

All MASs express the zinc-finger protein Stripe (Fig. 2A) (18, 25). Beginning at stage 13 of embryogenesis, slit is also expressed at the subset of MASs that lies along the segment

Howard Hughes Medical Institute, Department of Molecular and Cell Biology, 519 Life Sciences Addition, University of California, Berkeley, CA 94720, USA.

*Present address: Exelixis, 170 Harbor Way, Post Office Box 511, South San Francisco, CA 94083–0511, USA.

†To whom correspondence should be addressed.